



# Numerical simulation of P and S wave propagation in porous and low porosity carbonate rocks: laboratory tests, automatic P and S waves detection and FLAC3D simulation

Ali Besharatinezhad<sup>1</sup> · Ákos Török<sup>1</sup>

Received: 16 December 2022 / Accepted: 7 July 2024 / Published online: 19 July 2024  
© The Author(s) 2024

## Abstract

This study presents laboratory measurements of P and S wave velocities of two carbonate rocks (porous limestone and yellow cemented limestone). The experimental results were validated and compared with the numerical simulation outputs using the 3D Fast Lagrangian Analysis of Continua software (FLAC3D). The main aim of this study is to evaluate the effect of frequency and mode of emission on ultrasonic pulse velocity (UPV) by applying an automatic method for the determination of P and S wave velocities. Based on the results, automatic detection of UPV can provide reliable outputs. The difference between numerical simulation results and laboratory measurement in terms of P and S wave velocities was, on average, around 7%, suggesting the applicability of the automatic detection method. Our study implies less noise in the perfect shear (PS) mode than in the single zone (SZ) emission mode. In summary, higher frequencies and the PS mode of emission are recommended.

## Highlights

- The applicability of the numerical method in ultrasonic wave propagation was proven.
- Automatic detection of UPV needs to be adjusted based on the type of transducer.
- Increasing transducer frequency causes a more straightforward form of wave emission with a lower amount of noise.
- The perfect shear (PS) emission mode yielded more precise results than the single zone (SZ) emission mode and decreased the extra noise propagation.

**Keywords** FLAC3D · Ultrasonic propagation · S wave · Automatic detection · Limestone · Emission mode

## Introduction

The ultrasonic transmission technique is one of the non-destructive methods for evaluating rocks' physical and mechanical properties. This method is fast and cost-effective compared to classic techniques (i.e., uniaxial loading test) and eliminates time-consuming and extensive sample preparation compared with field experiments (Uyanik et al. 2019; Vasconcelos et al. 2008). It can be used for studying

samples and deriving P and S waves velocities and evaluating the effect of (a) stress, (b) changes in water content, (c) salt crystallization, (d) weakness planes such as schistosity and discontinuities, and (e) temperature in the rocks and can be compared to results that were obtained with other test methods (Bauer et al. 2016; Brotóns et al. 2013; Fathollahy et al. 2021; Moomivand et al. 2021a, b; Motra et al. 2018; Příkryl 2001; Rabat et al. 2021, 2023; Rahman and Sarkar 2021; Rozgonyi-Boissinot et al. 2021; Yang et al. 2021; Freire-Lista et al. 2016, 2022). These techniques are becoming more common in geotechnical and civil engineering because they are non-destructive and easy to apply (Sharma and Singh 2008; Vasanelli et al. 2015; Vasconcelos et al. 2008; Parisi and Augenti 2017; Micelli and Cascardi 2020). Determining P wave velocity is easy to obtain because it has been less affected by noise. On the other hand, analyzing S wave velocity faces many difficulties due to noise, P wave

✉ Ákos Török  
torok.akos@emk.bme.hu

<sup>1</sup> Department of Engineering Geology and Geotechnics, Faculty of Civil Engineering, Budapest University of Technology and Economics, Muegyetem rkp 3, Budapest H-1111, Hungary

velocity, human errors, the frequency of ultrasonic devices, and mode of emission. Two methods do detect pulse waves: manual and automatic detection of P and S wave velocities. Manual picking of the first onset of P and S waves demands experience and skill, and there is always a possibility of errors due to noise, human errors, and experimental situations (e.g., temperature, sample preparation, the contact area between transducers and sample), etc. The automatic detection of elastic wave velocities was suggested as an alternative method for UPV detection (Sarout et al. 2009; Acciani et al. 2010; Benavente et al. 2020).

Trying to remove a large part of noise with small amplitude, Mousavi et al. (2016) presented a combination of synchro-squeezed continuous wavelet transform (SS-CWT) and wavelet de-noising. It was based on SNR (Signal Noise Ratio) improvement. Another approach is the short-term average – long-term average (STA/LTA) ratio (Aster et al. 1998). This method was used for P wave determination, and it was based on signal energy densities. To overcome the limitation of the STA/LTA method, e.g., only covering signals with low amplitude, a modified energy ratio (MER) approach based on STA/LTA was presented. MER determines the first P wave arrival time based on the variation of energy densities of the signal. The MER method provides more reliable results for data with a low SNR than the STA/LTA method (Lee et al. 2017). This approach successfully reduces the effect of the amplitude of the signal, which was one of the key factors in the first onset of wave determination. However, these procedures could precisely determine P wave velocity when the main signal had low noise. Still, when the signal was highly contaminated with noise, these methods did not perform properly. For these reasons, an automatic algorithm for P and S wave's first onset determination was proposed by Benavente et al. (2020). This method was based on a wavelet analysis to improve SNR and the detection of output pulses to identify the first pulse of P and S waves. Other studies (e.g., Sarout et al. 2009) used the input pulse frequency to analyze a frequency band. Benavente et al. (2020) found that the discrepancy between manual and automatic detection of the P wave is 0.7%. S wave is mostly interlocked with P wave and other noise, and therefore, it causes inaccurate identification of arrival time (Wang et al. 2009; Acciani et al. 2010; Huang et al. 2021). Some researchers indicated that while the propagation of noise depends on the mode of emission (Éthier and Karray 2011; Huang et al. 2021), the size of the transducer and the frequency also have a significant influence on output data (Basu and Aydin 2006; Shirole et al. 2020; Wang et al. 2019). To analyze these parameters and their effect on UPV, numerical simulation has been considered a fast and reliable method for determining the strength parameters of rocks, crack detection, and investigation through wave

propagation in different media. With the help of the MATLAB programming language, Chen et al. (2017) simulated wave propagation through stones using the high-order staggered-grid finite difference method (second-order in the time domain and fourth-order in the space domain). The effect of frequency in a numerical approach was not significant and with increasing frequency, the velocity did not experience considerable changes. A positive logarithmic relationship between frequency and velocity was found compared with experimental results. Yorikov et al. (2019) applied the FEM (finite element method) to simulate S wave transmission through rocks in order to evaluate the applicability of S transducers for P and S wave velocity determination. They revealed that P wave transducers had a higher measured velocity than S wave transducers. They also observed that S wave transducers produced both P and S waves. Huang et al. (2021) simulated wave propagation through rocks with the help of FEM. They observed different types of waves, including Rayleigh wave, vertical S wave, head wave, and P wave. P wave was the first wave that arrived at the end of the model. The diameter of the transducers was 16 mm. The edges produced edge P waves, and these reflected waves directly affected S wave velocity. They found out that the dominant wave for the P wave transducer was a direct plane P wave, and for the S wave transducer, it was a direct plane S wave. Liu et al. (2015) modelled the propagation of ultrasonic waves through pipes for crack detection with the help of FEM. They found that choosing the proper frequency has an important effect on crack detection, and lower frequencies can better identify cracks. However, FEM is one of the most popular methods in civil engineering, but in terms of ultrasonic modelling, it is slow. For high frequencies, the wavelength is tiny, and to have a reliable result, the number of elements in FEM should be large enough to meet the requirement of choosing a proper mesh system based on frequency (Kundu et al. 2010). Éthier and Karray (2011) presented a FLAC simulation to examine wave propagation in a Bender Element (BE) test. They considered two emission modes for the S transducer, including single point shear and perfect shear. It was revealed that the perfect shear mode of emission waves was more planar compared to the single point shear mode of emission, and consequently, its interpretation was easier and more precise. To understand the wave propagation path due to blasting in the ground, a simulation of stress waves was performed in FLAC3D (Fast Lagrangian Analysis of Continua in Three-Dimensions, by Itasca Consulting Group Inc.) by Resende et al. (2014). The applicability of DEM (Discrete Element Modeling) was proven by comparing numerical data with experimental results. In comparison with FEM, this method is faster, and the results are reliable. The effect of emission mode on the main results and choosing a well-adapted automatic method

for determining UPV based on the type of transducers were less considered by researchers. It is linked to the difficulties in UPV detection and many uncertainties about the influence of the transducer on wave propagation and, consequently, the P and S wave velocities.

In this study, limestone was chosen as it has been widely used in many countries and historic structures. It includes restoration material for the Acropolis Greece (Ksinopolou et al. 2022), the Anahita Temple of Kangavar in Iran (Barnoos et al. 2022), limestone masonry at the Eski-Kermen Archeological Site in Crimea, Russia (Rudenko et al. 2023), Egyptian limestone monuments (El Badghady et al. 2019), the monument of Francesco III d'Este in Italy (Gherardini and Sirocchi 2022), historical monuments in France such as Notre-Dames de Paris (Praticò et al. 2020), and Basilica Saint-Denis (Gavino et al. 2004), built heritage in Oxford (Wilhelm et al. 2021), in Ljubljana, Slovenia (Kramar et al. 2011), in cities of Belgium (Fobe et al. 1995; De Kock et al. 2017) monuments in rural area of Hungary and Germany (Török et al. 2011) which indicate its importance for further consideration. The Geotron (Consonic C2-GS Geotron Elektronik) instrument propagated ultrasonic waves in porous limestone (travertine) and yellow cemented limestone. Wave propagation through samples was simulated numerically with the help of FLAC3D software. S and P wave velocities were determined automatically based on the method described by Benavente et al. (2020). It is worth noting that the automatic detection of wave velocity was adjusted based on the ultrasonic device and transducer. The results of the experimental approach were compared and

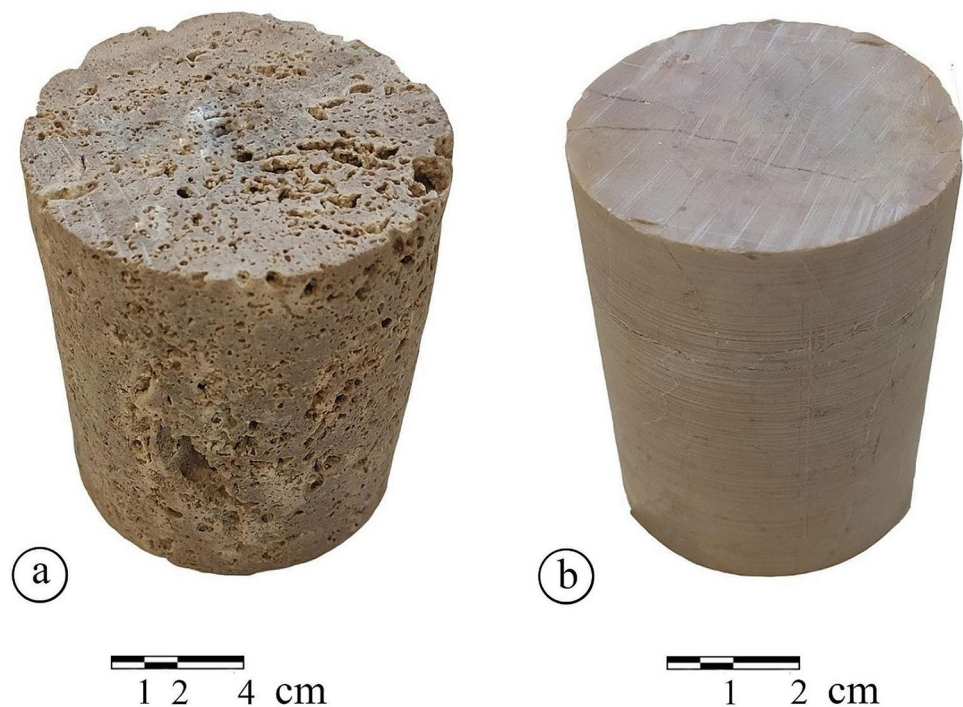
validated with the numerical simulation results. The results suggest an adjusted automatic UPV detection method with PS emission mode for precise detection of the first onset of P and S wave velocities.

## Materials and methods

### Materials

Two types of common limestone (porous travertine and cemented limestone) were used for the pulse velocity tests (Fig. 1). The tested travertine is a Pleistocene deposit with high porosity. The larger, elongated pores often follow the micro-fabric, forming a laminated texture. Smaller calcified plant fragments of phytoclasts are also detectable. It has a phytothermal boundstone and pyhtoclastic boundstone micro-fabric. The lithology was previously described in detail (Török 2008). Travertine is a widespread stone; it is known from more than 300 sites only in Europe (Pentecost 2005), but quarries have been exploited from antiquity in Europe and Asia. Well-known historical sites such as Hieropolis in Turkey, buildings like the Colosseum of Rome, and recent symbolic structures such as the Getty Centre in Los Angeles were built from travertine. The cemented micro-crystalline limestone differs from travertine. It is also composed of calcite but has very low porosity (0.3%) and has micro-metre scale pores. Its micro fabric is bioclastic wackestone. The studied specimen is a marine limestone, representing Jurassic carbonates of the Alpine system.

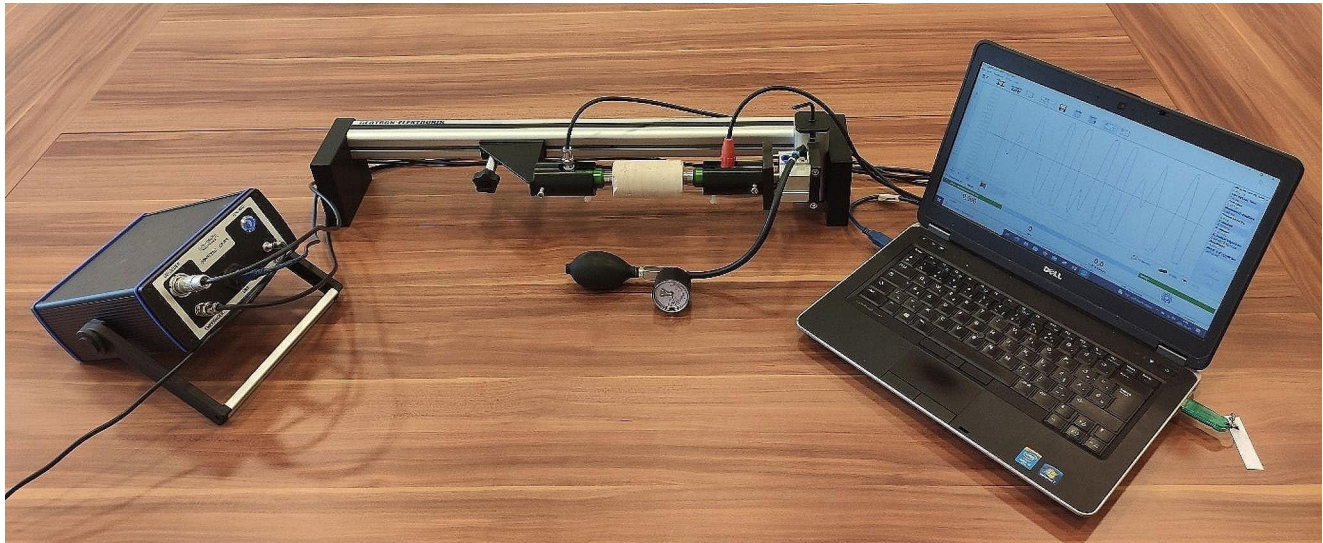
**Fig. 1** Tested carbonate rocks: (a) porous limestone (travertine); (b) yellow cemented limestone





**Table 1** Physical and mechanical properties of the samples

	Density (g/cm <sup>3</sup> )	Height (H) (mm)	Diameter (D) (mm)	porosity (%)	UCS (MPa)	Tensile strength (MPa)	E (GPa)	Poisson ratio ( $\nu$ )
Porous limestone (travertine)	2.136	83.53	71.53	8.3	60	5.7	12.4	0.36
Yellow cemented limestone	2.665	83.24	44.52	0.3	80	7.2	23.0	0.231

**Fig. 2** Ultrasonic sound testing device (Consonic C2-GS Geotron Elektronik instrument)

Cemented low porosity micro-crystalline limestones are known in many countries in Europe and worldwide, and they have various colours and geological ages (Siegesmund and Török 2011). The mechanical properties of the studied samples were measured in laboratory conditions (Table 1).

### Laboratory testing

Ultrasonic velocities of the sample were measured with the help of the Geotron (Consonic C2-GS Geotron Elektronik) instrument (Fig. 2). A direct transmission method was considered for experimental measurement. In this method, transducers were placed opposite each other, and ultrasonic waves can directly propagate from emitter to receiver. S transducers (UP-SW) with the optimal frequency of 80 kHz based on the manufacturer's recommendation in the Geotron manual were used to excite S waves. However, S transducers are designed to produce S waves, but the propagation of longitudinal waves during S wave excitation is unavoidable. Consequently, S transducers produce both P and S waves (Lebedev et al. 2011; Yurikov et al. 2019), but the primary function of these S transducers is to increase SNR for S waves with attenuating longitudinal waves. Ultrasonic measurement was performed five times for each sample in dry conditions. P and S waves were evaluated from Geotron experimental results with an excitation voltage of 50mV

and 2 V, respectively. No coupling between transducers and sample was used during ultrasonic measurement, and transducers were directly attached to the samples.

### Data processing

- The Benavente et al. (2020) method for automatic detection of UPV has been implemented in this study. The process map of the steps has been summarized in Fig. 3. The method has been adjusted based on the ultrasonic device (Geotron) signals to yield precise results. This adjusted method has been used in another paper by the authors (Rozgonyi-Boissinot et al. 2021), and its applicability has been proven. Due to the high SNR of the Geotron device, the first onset of P wave velocity was detected without applying filters. For P wave velocity calculation, the absolute value of pulses has been taken and normalized based on the maximum value. The first pulse where a normalized value is more than 1% has been taken as the first pulse of P wave velocity, and the corresponding time of the pulse was used for P wave velocity calculation (Fig. 4). Based on the Geotron manual, the first negative pulse should be at least 50% of the maximum amplitude. For amplitude 50mv, the first negative pulse of signals satisfied the manual

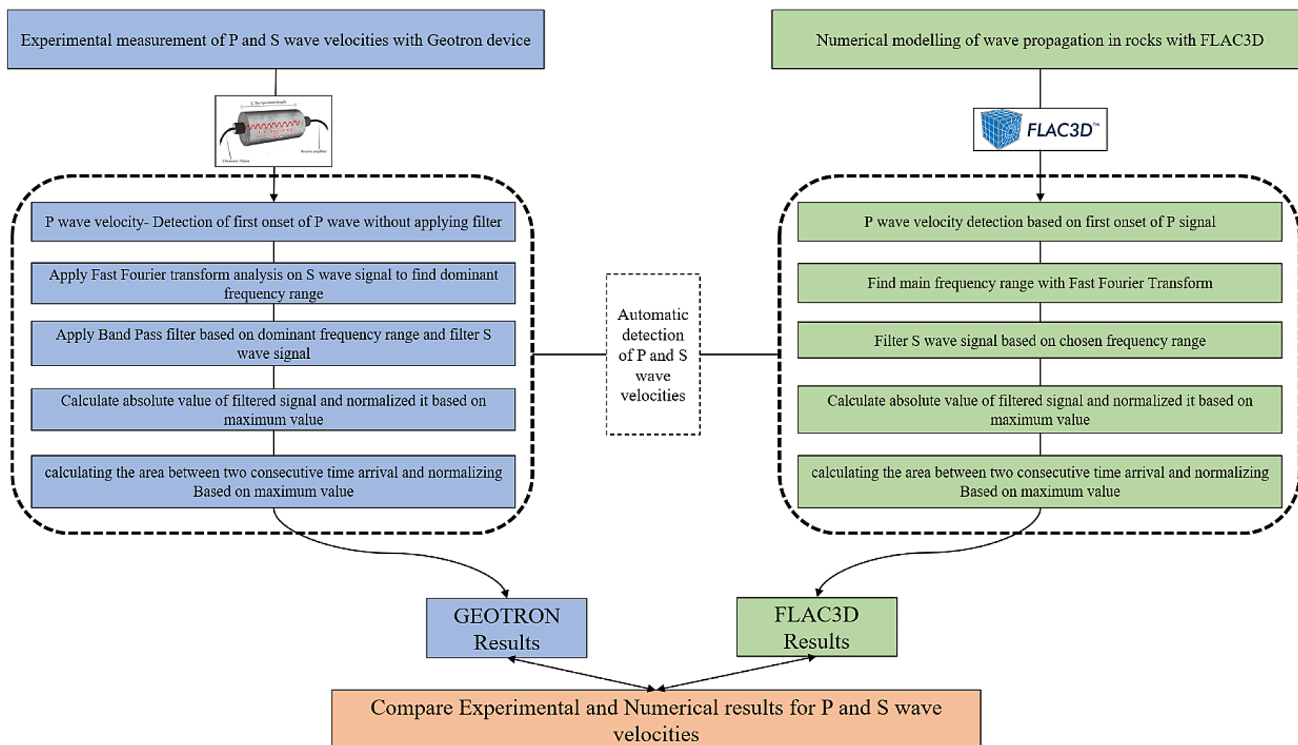


Fig. 3 Process map of P and S wave velocities measurement and calculations with numerical and experimental methods

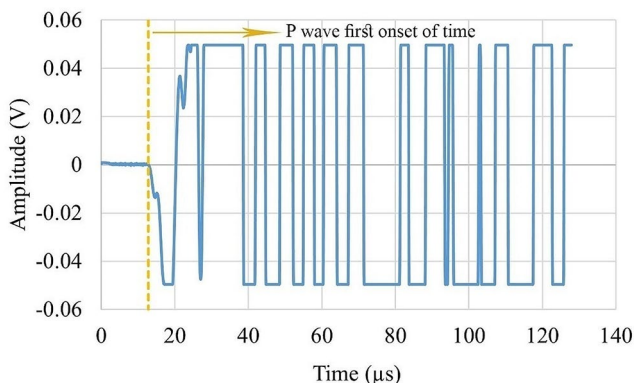


Fig. 4 Graphs representing wave detection methods of P waves with amplitude = 50mV

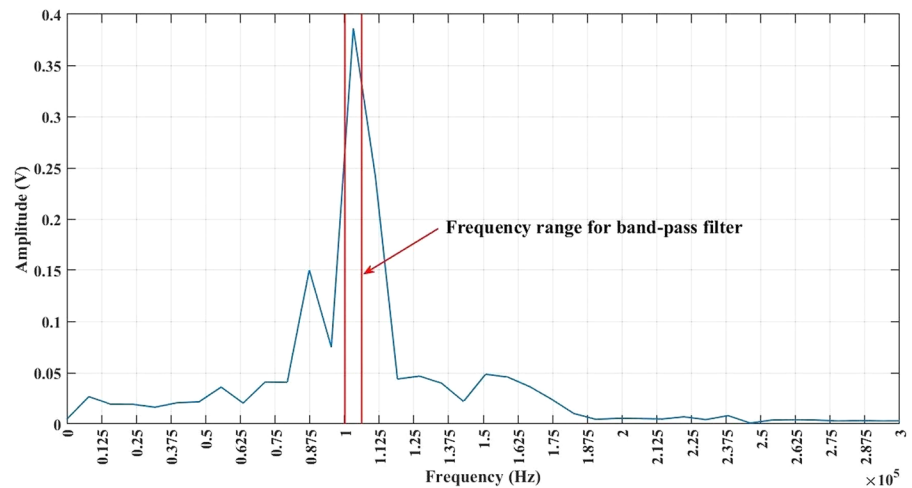
requirement. Please note this step is necessary due to the determination of P wave velocity. However, due to the small number of noises in the signal, no filter has been applied to the signal. Verifying this step is easy as the first onset of the wave can be determined approximately with visual detection.

- In the FLAC3D model, elastic waves were propagated via the specimens, and the software calculated the output, while in the experiments, the samples were measured using a GEOTRON device. In the latter one, using sample uncertainties such as human error, existing heterogeneities in pore system and texture, and imperfect

sample surface affected the results. In the FLAC3D model, there were no other noises, making it easier to post processing the signal. The experimental and numerical approach results were extracted and analysed with the same method. Finally, the P and S waves extracted from the results were compared.

- Due to the type of the transducer and high SNR value, the signals were considered almost clean, and we did not have to apply signal pre-processing, including removing low-frequency disturbances of the signal, signal denoising, and elimination of high-frequency oscillation. In the first step, a Fast Fourier Transform analysis has been implemented on the signal to derive the frequency of the maximum amplitude (Fig. 5). Fourier Transform analysis will help us to determine the dominant frequency and filter noises. In the second step, the bandpass filter within the range of  $\pm 3000$  Hz was applied to the signal (Fig. 6a). It is worth noting that this range was chosen after the comparison with other ranges conducted for S wave filtering in the band-pass filter. A band-pass filter allows frequencies within a specific range to pass while attenuating frequencies outside that range (MATLAB manual, 2019). In the third step, the absolute value of the filtered signal has been taken and normalized based on the maximum pulse value (Fig. 6b). The fourth step consists of calculating the area between two consecutive time arrival and normalizing concerning its maximum

Fig. 5 FFT graph with a band-pass range



value (Fig. 6c). From Fig. 5c, the first column will represent the first arrival time for the calculation of S wave velocity. Based on Benavente et al. (2020) and Rozgonyi-Boissinot et al. 2021 these steps will help us to determine the first onset of S-wave velocity as compared to P-wave velocity; this recognition is more difficult.

### FLAC3D modelling

Elastic wave propagation in rocks was simulated with the help of FLAC3D software. The input parameters for FLAC3D are presented in Table 2. The samples, whose dimensions are presented in Table 1, are cylindrical. The geometry and mesh system of the model are presented in Fig. 7a and b. At least 160,000 zones were created for the models. Grid points were fixed at x, y, and z-direction on both sides of the models. The material for the samples was assumed elastic, and their elastic mechanical parameters (Table 2) were applied to the FLAC3D model. In this model, we supposed that there are no micro-cracks, textural heterogeneities, or material properties that are uniform for the entire length of the modelled specimen. The heterogeneity was considered using input parameters such as density and modulus of elasticity. Please note that the model was calculated for non-pressurised conditions, which means there was no loading or unloading applied to the model. A sinusoidal pulse wave was applied to the model. The wave propagation in three frequencies (80, 160, and 240 kHz) was calculated. It was applied horizontally (in the x-direction) through the sample (Fig. 7c). It was assumed that the source transducer produced a wave parallel to the horizontal surface of the samples. The receiver transducer was placed on the other side of the sample and recorded x velocity changes (Fig. 7). At first, the model was statically analyzed. Then displacements and velocities were set to zero in x, y, and

z-direction. Then, dynamic analysis was performed for the stabilized model. The velocity and displacement changes in the x and y direction were recorded. The x velocity taken from the monitoring point at the end of the sample was normalized to its maximum value.

P and S waves' first arrival time and velocities were calculated automatically based on the adjusted Benavente et al. (2020) method used in the experimental part. The P wave velocity was calculated based on the first wave arrival, without filtering (orange dashed line in Fig. 8). For the S wave first arrival determination, the signal was filtered with a band-pass filter, and then the first onset of the S wave was determined (green dashed line in Fig. 8).

### Results

The wave propagation through the sample was conducted for two different emission modes that are shown in Fig. 9. In the single zone (SZ) mode of emission, the wave propagated through the sample from a small circular area with a diameter of 18 mm, while for perfect shear (PS) mode of emission wave propagated in an area equal to the width of the sample.

X-velocity contours in the xy-section for PS and SZ mode of emission are visualised in Figs. 10 and 11) and Figs. 12 and 13, respectively. These contours were arranged for three different frequencies (80, 160, and 240 kHz) and three different sets of time ( $t_{10\%}$ ,  $t_{50\%}$ , and  $t_{90\%}$ , which are 10, 50 and 90% of S wave arrival time, respectively) based on S arrival time for yellow cemented limestone (21.50  $\mu\text{s}$ ) and for porous limestone (31.77  $\mu\text{s}$ ). The perfect shear (PS) emission mode yielded a more straightforward wave propagation form (Figs. 10 and 11), and consequently, the interpretation of signals is easier and more precise. The dominant waveform was the direct plane S wave (DS). On the other hand, the SZ emission mode caused different wave types from the

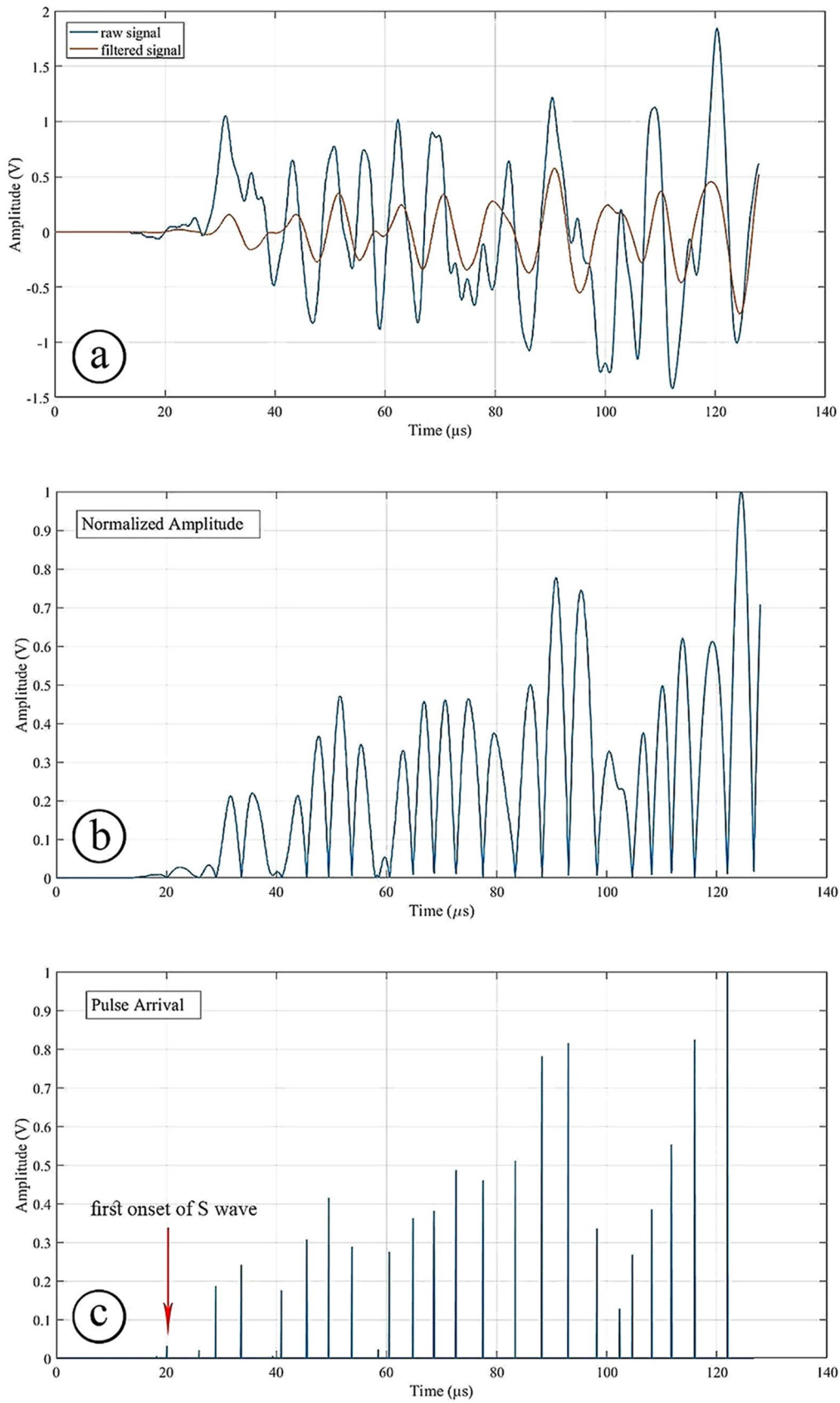


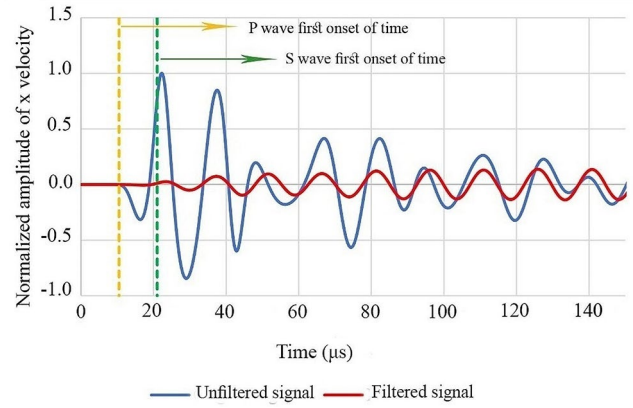
**Fig. 6** Main steps for automatic detection of S wave velocity: (a) raw and filtered signal with band-pass filter; (b) absolute values of normalized signal; (c) pulse arrival



**Table 2** Input parameters in FLAC3D

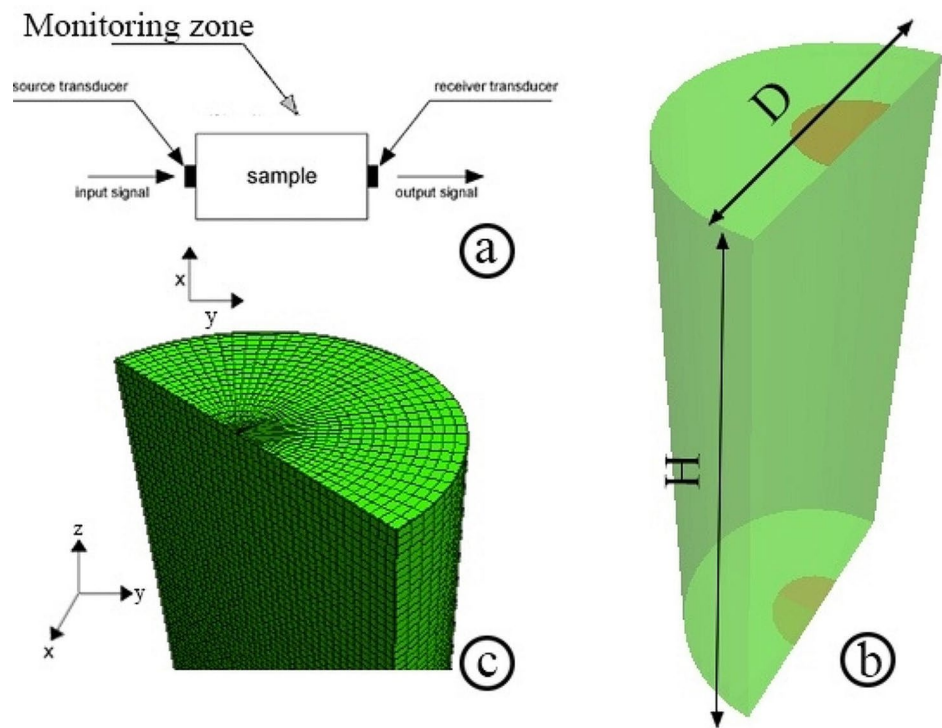
	Diameter (mm)	Height (m)	Poisson ratio (ν)	E (GPa)
Porous limestone (travertine)	71.53	83.53	0.360	12.4
Yellow cemented limestone	44.52	83.24	0.231	23.0

initial stages of wave propagation (Figs. 12 and 13). These waves in numerical and experimental methods can precede P and S waves and influence the interpretation of the output signal. For the PS mode of emission, wave propagation for both types of stones followed the same trend, and both presented a more planar S wave emission with increasing frequency (Figs. 10 and 11). However, for the SZ mode of emission, porous limestone had more wave dispersion than

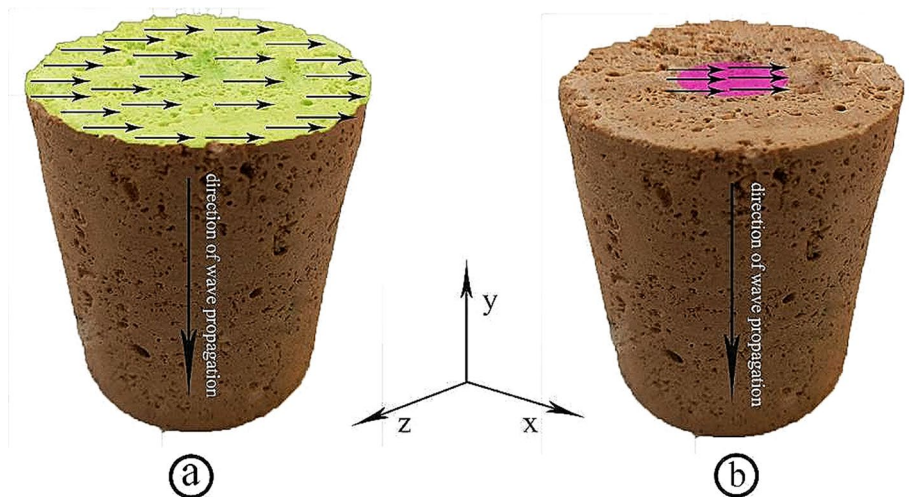


**Fig. 8** Identification of wave velocity from FLAC3D output signal

**Fig. 7** Laboratory testing and numerical modelling scheme: (a) sketch of wave propagation and sample; (b) monitoring points of transducers positions (in brown) and (c) mesh system in FLAC3D



**Fig. 9** Emission modes: (a) Perfect Shear (PS) and (b) Single Zone (SZ)





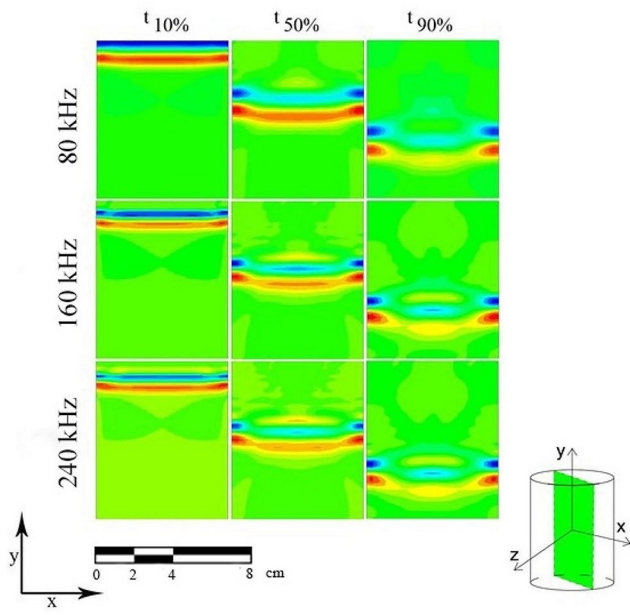


Fig. 10 X velocity contour for perfect shear (PS) emission mode for porous limestone (travertine)

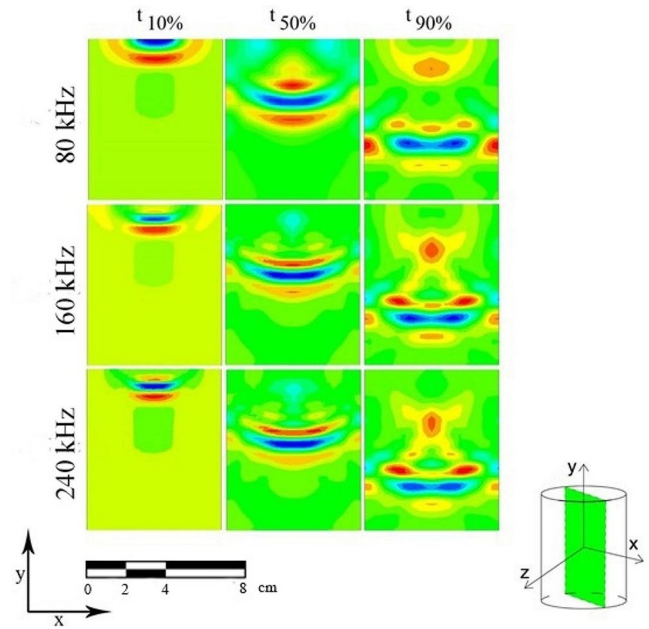


Fig. 12 X velocity contour for single zone (SZ) emission mode for porous limestone (travertine)

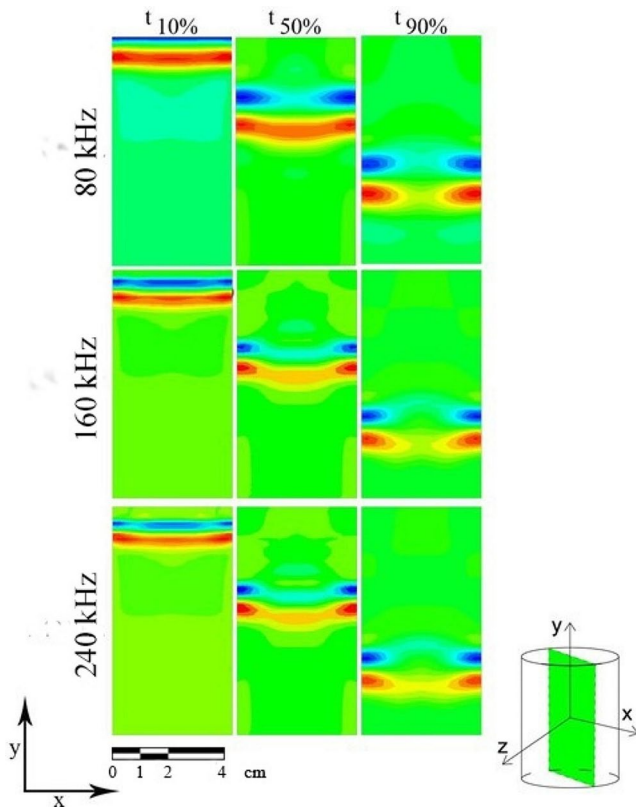


Fig. 11 X velocity contour for perfect shear (PS) emission mode for yellow cemented limestone

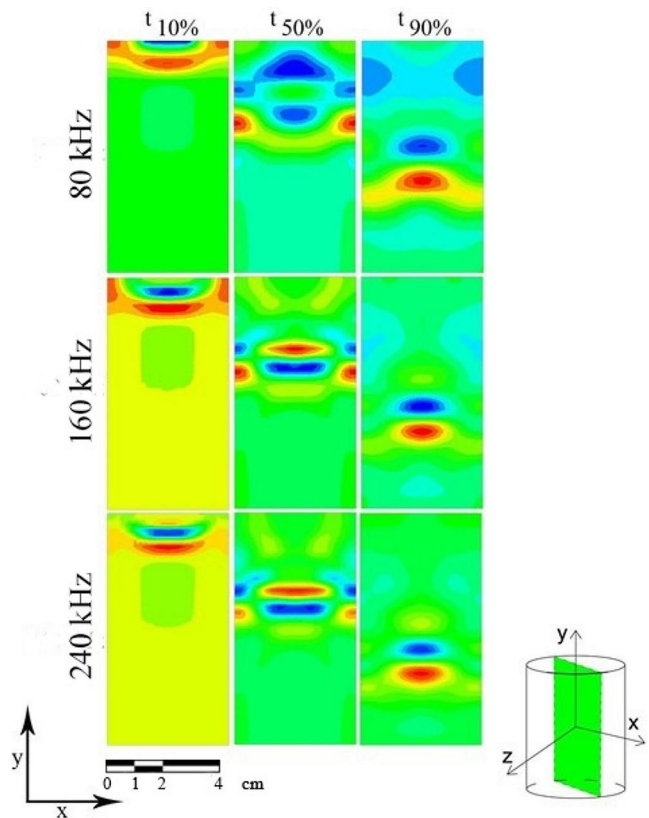
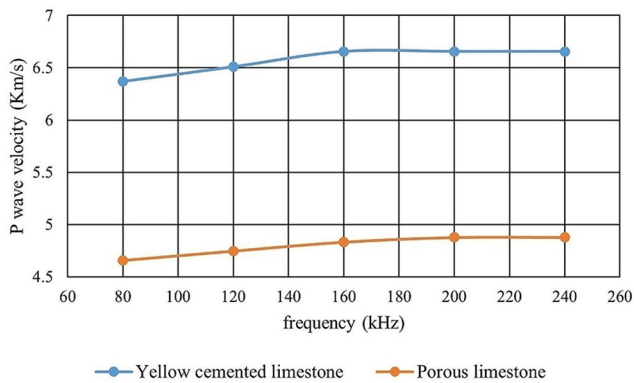


Fig. 13 X velocity contour for single zone (SZ) emission mode for yellow cemented limestone

**Table 3** The P and S wave velocities at different frequencies for the PS mode of emission

Wave type	Stone type	Frequency (kHz)				
		80	120	160	200	240
P wave velocity (km/s)	Yellow cemented limestone	6.371	6.510	6.656	6.656	6.656
	Porous limestone (travertine)	4.657	4.746	4.832	4.876	4.876
S wave velocity (km/s)	Yellow cemented limestone	3.872	3.925	4.087	4.111	4.122
	Porous limestone (travertine)	2.629	2.720	2.800	2.841	2.841



**Fig. 14** P wave velocity changes as a function of frequency for PS emission mode

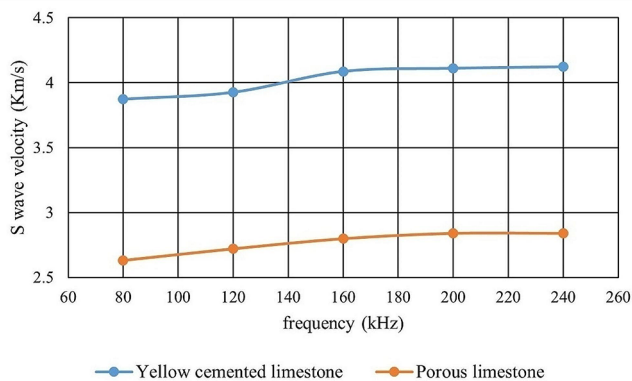


**Fig. 15** S wave velocity changes as a function of frequency for PS emission mode

cemented limestone. As frequency increased, the differences between wave propagation reduced (Figs. 12 and 13).

P and S wave velocities at different frequencies for PS mode of emission have been presented in Table 3. As observed previously, the frequency influenced the type of signal and the P and S wave velocities (Figs. 14 and 15). There was a steady increase in both P and S wave velocities with increasing frequency from 80 kHz to 240 kHz. P wave velocity was increased by 4.46 and 4.72% for yellow cemented and porous limestone, respectively (Fig. 14). S wave velocity was also raised by 6.47 for yellow cemented limestone and by 8.05% for porous limestone (Fig. 15). Please note. However, frequency should not have any effect on the results taken from an elastic model without any

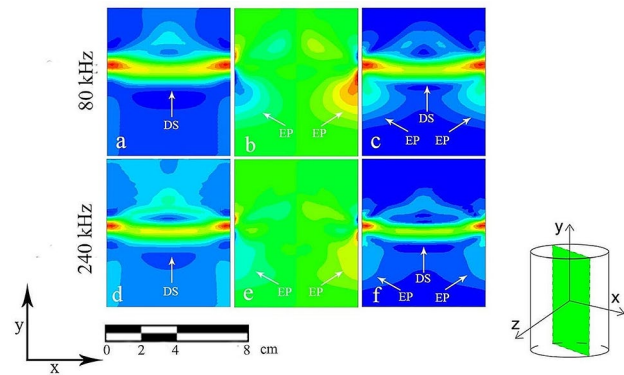


**Fig. 16** Transverse displacement (a,d), average displacement (b,e) and magnitude displacement (c,f) contours for PS transmission mode at  $t_{50\%}$  for porous limestone -travertine (DS: direct plane S waves; EP: edge P waves)

cracks. Still, as post processing and the results alongside with reflecting waves to the edge of the model due to the wave propagation will affect the results, different frequencies have been considered to analyze in which frequency the differences in the result will be negligible. Based on the results for frequencies higher than 160 kHz, the differences between velocities are negligible and less than 1.5%) The porous limestone experienced a higher increase than cemented limestone; however, the difference was insignificant. S waves were more sensitive to frequency changes. As frequency increased, the P and S wave velocities differences ( $\Delta P$  and  $\Delta S$ ) were decreased.

Normal, transverse and magnitude displacement contours for PS mode were plotted for porous and cemented limestone (Figs. 16 and 17). The P and S wave propagation trend was almost the same for both types of limestone. The standard displacement contours revealed the propagation of S waves. Due to a perfect shear transmission mode (PS), a direct plane S wave (DS) was emitted. As frequency increased (Figs. 16d and 17d), the shape of the S wave became more planar, and the presence of extra noise decreased.

A comparison of P and S wave velocities from numerical simulation and average P and S wave velocities from the Geotron instrument is presented in Table 4. It is important to note that in the FLAC3D simulation, samples were considered elastic, intact, and without cracks. Therefore, results from numerical simulation indicated P wave velocity

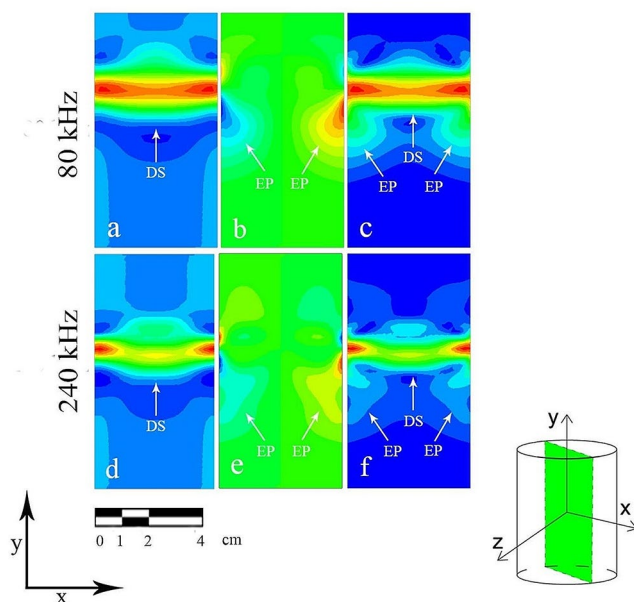


**Fig. 17** Transverse displacement (a,d), average displacement (b,e) and magnitude displacement (c,f) contours for PS transmission mode at  $t_{50\%}$  for yellow cemented limestone (DS: direct plane S waves; EP: edge P waves)

and S wave velocity for an intact stone with given elastic parameters. For these reasons, results from the numerical simulation were always expected to be higher than laboratory experiment results. Compared with Geotron results, P wave velocity and S wave velocity for numerical simulation increased by 8.4 and 4.3% for porous limestone, respectively. P wave velocity and S wave velocity increased by 5.1 and 7.8% for cemented limestone, respectively.

### Discussion

Although S wave emission will be expected based on the type of the transducer, from both numerical and experimental results, it has been proven that the emission of extra noise and P wave alongside the S wave is inevitable. Huang et al. (2020) observed the existence of different types of waves when the input signals propagated through the sample from a width that was smaller than the total width of the sample (e.g., signal point (SP) mode of emission and single zone (SZ) mode of emission). Therefore, the automatic determination of ultrasonic waves is always necessary to yield precise results in terms of P and S wave velocities

and reduce the negative effect of noise in the results (Huang et al. 2021). Benavente et al. (2020) proposed a reliable automatic method for UPV detection, which has been used in this study and adjusted based on the ultrasonic device. It is worth noting that while the accuracy of Benavente et al. (2020) for the detection of UPV was proven and taken for this study, due to different devices that had been used, the method should be adjusted and then implemented for the signal output from Geotron. In these studies, the accuracy of the results was affected by the input signal and the percentage of its contamination with noise. There was a lack of consideration of some of the main parameters influencing the input signal, such as mode of emission and frequency. However, Ethier et al. (2011) indicated that the mode of emission influences the form of wave propagation, and a proper choice of emission mode could reduce the negative effect of noise. Still, they also revealed that noise propagation due to reflection and diffraction could not be neglected. In this study, two types of emission modes, including PS and SZ mode of emission, were considered, and the importance of the mode of emission of the output signal was emphasized. The noise generated with these modes of emission can precede P and S waves arrival and cause significant errors in results, but choosing the proper mode of emission can reduce the negative effect of this extra noise and increase the accuracy of automatic detection of UPV. Arguably, for transducers with smaller diameters, the possibility of propagation of unwanted noise will increase due to reflection, the spherical form of P and S waves, etc. Acciani et al. (2010) observed surface wave; however, because the sample's width was large enough compared to the transducer width, extra noise due to the reflection of the received signal was not generated. The same result was observed by Huang et al. (2020), and as the diameter of the emitter increased, the propagation of extra unwanted noise like edge P and S waves decreased. The presence of edge P waves (EP) was obvious. However, these reflected edge P waves are not considered in comparison with big plane S waves. Still, their effect cannot be neglected (Ethier et al. 2011), and their velocity should be measured. Numerical simulation cannot reflect the contribution of these longitudinal waves (Huang et al. 2021), but the propagation of P waves with S transducers was proved in experimental studies (Lebedev et al. 2011; Yurikov et al. 2019) and in numerical simulations (Ethier et al. 2011; Nygren, 2011; Huang et al. 2021). The same results have also been observed in this study. It

**Table 4** P and S wave velocities were measured in the laboratory with a Geotron instrument, and the results of numerical simulations with FLAC3D

	Geotron instrument (Std. dev)		FLAC3D		Relative difference (%)	
	$v_p$ (km/s)	$v_s$ (km/s)	$v_p$ (km/s)	$v_s$ (km/s)	$v_p$	$v_s$
Porous limestone (travertine)	4.293 (0.114)	2.518 (0.132)	4.656	2.629	8.4	4.3
Yellow cemented limestone	6.058 (0.138)	3.589 (0.143)	6.371	3.872	5.1	7.8

can be concluded that the PS mode of emission mainly produces edge P wave (EP) and direct plane S wave (DS), and the presence of other noise is negligible. Chen et al. (2017) observed a positive correlation between ultrasonic velocity and frequency for experimental results, and the velocity did not experience significant changes due to increasing frequency. They concluded that the trend between frequency and ultrasonic velocity was more consistent for numerical results and proved that frequency dispersion in a numerical approach is negligible due to neglecting the effect of microcracks, clays, and other materials. Basu and Aydin (2006) showed that more reliable results are obtained by applying higher frequencies. So, it can be said that higher frequencies lead to better comparable results for different transducers and between numerical simulation and experimental results. Higher frequencies also increase the ability to detect changes in rocks due to weathering, pressure, etc. (Basu and Aydin 2006; Wang et al. 2019). It can be observed that as frequency increases, waveform tends to be more planar, and dispersion also decreases. The same result was observed by Ethier et al. (2011). But it is important to state that transducers with higher frequencies are recommended, but for those with high frequency (e.g. higher than 1 MHz), the dominant frequency does not change significantly, and because of the existence of inherent microcracks that filter signals at their low pass range, the sample only passing frequencies that are lower than its characteristic frequency (Shirole et al. 2020). In summary, frequency and emission mode (size of the transducer) significantly affect output signals (Basu and Aydin 2006; Ethier et al. 2011; Huang et al. 2021) and, consequently, on the interpretation of outputs. Porosity is another important parameter that may significantly influence P and S wave velocities. Porosity affects wave propagation and output signals, and as porosity increases, lower P and S wave velocities are reported (Iyare et al. 2021; Jamshidi et al. 2018). Numerical wave propagation simulation can help better understand the transducers' function at different types of samples, frequencies, and modes of emission. Moreover, approving the reliability of numerical modelling compared to experimental modelling can prove a simple and easy-to-use method for analyzing P and S wave velocities of rocks. It can be useful for calculating the mechanical parameters of rocks.

## Conclusions

1. The difference between experimental and numerical results was around 7%. It is considered as evidence of the applicability of this method. The numerical simulation validated the experimental approach and helped assess the effects of transducer frequency and emission mode on UPV results.
2. Samples were considered intact in the numerical simulation. This discrepancy between experimental and numerical results can be due to microcracks, voids, and any textural heterogeneity that negatively affects strength parameters and, consequently, modifies P and S wave velocity.
3. It was concluded that the perfect shear (PS) emission mode yielded more straightforward form signals compared with the single-zone (SZ) emission mode. PS mode also reduced the noise generation. Indeed, a combination of automatic wave interpretation for ultrasonic waves with numerical simulation in FLAC3D can be implemented as an easy alternative for choosing the proper transducer (in terms of frequency and diameter) and estimating pulse velocities.
4. The effect of frequency on signal form and P and S wave velocities were also investigated. An increase in frequency does not significantly affect P and S wave velocities; the signal form was more straightforward at higher frequencies. Higher frequencies ensure comparable results for different transducers and can be better used in comparing the results of numerical simulations and laboratory tests. A larger diameter for S transducers with higher frequencies provides more reliable S wave velocities.
5. In the SZ emission mode, porous limestone (travertine) experienced higher wave dispersion than cemented limestone. Therefore, using the PS mode of emission for both lithotypes is more beneficial. The use of the highest available frequency for the given transducer is recommended.
6. Based on the results, for this type of rock, frequencies higher than 160 kHz won't significantly affect P and S wave velocities.
7. Our analyses have proved that the mode of emission and frequency are the two main parameters controlling the accuracy of results.

**Acknowledgements** The research was partly funded by project no. BME-NVA-02 (Ministry of Innovation and Technology of Hungary from the National Research, Development and Innovation Fund), under the TKP2021 funding scheme. The same office provided support from a research grant to Á.T (ref. no. K 116532), which is also appreciated.

**Authors contribution** Both authors contributed to the writing of the manuscript. A.B., Á.T: Conceptualization; A.B: Methodology, Software; A.B., Á.T.: Writing, original draft preparation and revision. Á.T.: Supervision, Validation and Funding.

**Funding** Open access funding provided by Budapest University of Technology and Economics.



## Declarations

**Conflict of interest** The authors declared that they have no known competing financial interests or personal relationships that could have appeared to influence the study reported in this article.

**Open Access** This article is licensed under a Creative Commons Attribution 4.0 International License, which permits use, sharing, adaptation, distribution and reproduction in any medium or format, as long as you give appropriate credit to the original author(s) and the source, provide a link to the Creative Commons licence, and indicate if changes were made. The images or other third party material in this article are included in the article's Creative Commons licence, unless indicated otherwise in a credit line to the material. If material is not included in the article's Creative Commons licence and your intended use is not permitted by statutory regulation or exceeds the permitted use, you will need to obtain permission directly from the copyright holder. To view a copy of this licence, visit <http://creativecommons.org/licenses/by/4.0/>.

## References

- Acciani G, Fornarelli G, Giaquinto A, Maiullari D (2010) Nondestructive evaluation of defects in concrete structures based on finite element simulations of ultrasonic wave propagation. *Nondestructive Test Evaluation* 25(4):289–315. <https://doi.org/10.1080/10589751003658057>
- Aster RC, Young C, Withers M, Aster R, Beiriger J, Harris M, Moore S, Trujillo J (1998) A comparison of select trigger algorithms for automated global seismic phase and event detection. *Bulletin of the Seismological Society of America* (Vol. 88, Issue 1)
- Barnoos V, Shekofteh A, Oudbashi O (2022) Experimental evaluation of the consolidation treatments of low porosity limestone from the historic monument of the Anahita Temple of Kangavar, Iran. *Archaeol Anthropol Sci* 14(4):63. <https://doi.org/10.1007/s12520-022-01536-z>
- Basu A, Aydin A (2006) Evaluation of ultrasonic testing in rock material characterization. *Geotech Test J* 29(2):117–125. <https://doi.org/10.1520/gtj12652>
- Bauer A, Bhuiyan MH, Fjær E, Holt RM, Lozovyi S, Pohl M, Szczyk D (2016) Frequency-dependent wave velocities in sediments and sedimentary rocks: Laboratory measurements and evidences. *Lead Edge* 35(6):490–494. <https://doi.org/10.1190/le35060490.1>
- Benavente D, Galiana-Merino JJ, Pla C, Martínez-Martínez J, Crespo-Jiménez D (2020) Automatic detection and characterization of the first P- and S-wave pulse in rocks using ultrasonic transmission method. *Eng Geol* 266. <https://doi.org/10.1016/j.enggeo.2020.105474>
- Brotóns V, Tomás R, Ivorra S, Alarcón JC (2013) Temperature influence on the physical and mechanical properties of a porous rock: San Julian's calcarenite. *Eng Geol* 167:117–127. <https://doi.org/10.1016/j.enggeo.2013.10.012>
- Chen Q, Yao G, Zhu H, Tan Y, Xu F (2017) Numerical simulation of ultrasonic wave transmission experiments in rocks of shale gas reservoirs. *AIP Adv* 7:015205. <https://doi.org/10.1063/1.4974749>
- De Kock T, Turmel A, Fronteau G, Cnudde V (2017) Rock fabric heterogeneity and its influence on the petrophysical properties of a building limestone: Ledestone (Belgium) as an example. *Eng Geol* 216:31–41. <https://doi.org/10.1016/j.enggeo.2016.11.007>
- Ethier Y, Karray M, Lefebvre G (2011) Simulations of elastic wave propagation using FLAC to optimize the measurement of Shear wave velocity in the laboratory. *Continuum and Distinct Element Numerical Modeling in Geomechanics*, Minneapolis, Itasca International Inc, Paper 08–11
- Fathollahy M, Uromeihy A, Riahi MA, Zarei Y (2021) P-Wave Velocity calculation (PVC) in Rock Mass without Geophysical-Seismic Field measurements. *Rock Mech Rock Eng* 54(3):1223–1237. <https://doi.org/10.1007/s00603-020-02326-6>
- Fobe B, Vleugels GJ, Roekens EJ, Hermosin B, Ortega-Calvo J, Del Junco AS, Van Grieken R, Saiz-Jimenez C (1995) Organic and inorganic compounds in limestone weathering crusts from cathedrals in southern and western Europe. *Environ Sci Technol* 29:1691–1701
- Freire-Lista DM, Fort R, Varas-Muriel MJ (2016) Thermal stress-induced microcracking in building granite. *Eng Geol* 206:83–93. <https://doi.org/10.1016/j.enggeo.2016.03.005>
- Freire-Lista D, Gonçalves G, Vazquez P (2022) Weathering detection of granite from three asynchronous historical quarries of Sabrosa municipally (North Portugal). *J Cult Herit* 58:199–208. <https://doi.org/10.1016/j.culher.2022.10.008>
- Gavino M, Hermosin B, Vergès-Belmin V, Nowik W, Saiz-Jimenez C (2004) Composition of black crust from the Saint Denis Basilica, France as revealed by gas chromatography—mass spectrometry. *J Sep Sci* 27:513–523
- Gherardini F, Sirocchi S (2022) Systematic integration of 2D and 3D sources for the virtual reconstruction of lost heritage artefacts: the equestrian monument of Francesco III d'Este (1774–1796, Modena, Italy). *Herit Sci* 10(1):96. <https://doi.org/10.1186/s40494-022-00711-8>
- Huang X, Di B, Wei J, Shuai D, He L (2021) Finite-element analysis of noise preceding the arrival of S-Wave in Ultrasonic measurements of Rock velocities. *IEEE Trans Ultrason Ferroelectr Freq Control* 68(3):742–752. <https://doi.org/10.1109/TUFFC.2020.3011958>
- Iyare UC, Blake OO, Ramsook R (2021) Estimating the Uniaxial Compressive Strength of argillites using Brazilian Tensile Strength, Ultrasonic Wave velocities, and Elastic properties. *Rock Mech Rock Eng* 54(4):2067–2078. <https://doi.org/10.1007/s00603-020-02358-y>
- Jamshidi A, Zamanian H, Zarei Sahamieh R (2018) The Effect of Density and Porosity on the correlation between Uniaxial Compressive Strength and P-wave velocity. *Rock Mech Rock Eng* 51(4):1279–1286. <https://doi.org/10.1007/s00603-017-1379-8>
- Kramar S, Mladenović A, Pristacž H, Mirtič B (2011) Deterioration of the black Drenov Grič limestone on historical monuments (Ljubljana, Slovenia). *Acta Carsologica* 40(3). <https://doi.org/10.3986/ac.v40i3.60>
- Kundu T, Placko D, Rahani EK, Yanagita T, Dao CM (2010) Ultrasonic field modeling: a comparison of analytical, semi-analytical, and numerical techniques. *IEEE Trans Ultrason Ferroelectr Freq Control* 57(12):2795–2807. <https://doi.org/10.1109/TUFFC.2010.1753>
- Lebedev M, Bóna A, Pevzner R, Gurevich B (2011) Elastic anisotropy estimation from laboratory measurements of velocity and polarization of quasi-P-waves using laser interferometry. *Geophysics* 76(3). <https://doi.org/10.1190/1.3569110>
- Lee M, Byun J, Kim D, Choi J, Kim M (2017) Improved modified energy ratio method using a multi-window approach for accurate arrival picking. *J Appl Geophys* 139:117–130. <https://doi.org/10.1016/j.jappgeo.2017.02.019>
- Liu F, Lu Y, Lin F, Wang Z, Li F, Bai Y (2015) Numerical simulation of nonlinear ultrasonic guided waves for micro-cracking detection in pipelines. *Proceedings of SMAR2015, the 3rd Conference on Smart Monitoring, Assessment and Rehabilitation of Civil Structures*, Dubendorf Switzerland, EMPA, Swiss Federal Laboratories for Materials Science and Technology, 1–8
- Micelli F, Cascardi A (2020) Structural assessment and seismic analysis of a 14th century masonry tower. *Eng Fail Anal* 107. <https://doi.org/10.1016/j.engfailanal.2019.104198>

- Moomivand H, Maarefvand P, Moomivand H (2021a) A new empirical Approach to Assess Wave velocities and Dynamic Elastic properties of several models of jointed rock before and after grouting. *Rock Mech Rock Eng* 54(12):6439–6455. <https://doi.org/10.1007/s00603-021-02625-6>
- Moomivand H, Moomivand D, Nikrouz R, Azad R (2021b) Development of a new empirical relation to assess P-wave velocity anisotropy of Rocks. *Geotech Geol Eng*. 40:1537–1550. <https://doi.org/10.1007/s10706-021-01983-w>
- Motra HB, Mager J, Ismail A, Wuttke F, Rabbel W, Köhn D, Thorwart M, Simonetta C, Costantino N (2018) Determining the influence of pressure and temperature on the elastic constants of anisotropic rock samples using ultrasonic wave techniques. *J Appl Geophys* 159:715–730. <https://doi.org/10.1016/j.jappgeo.2018.10.016>
- Mousavi SM, Langston CA, Horton SP (2016) Automatic microseismic denoising and onset detection using the synchrosqueezed continuous wavelet transform. *Geophysics* 81(4):341–355. <https://doi.org/10.1190/GEO2015-0598.1>
- Parisi F, Augenti N (2017) Structural failure investigations through probabilistic nonlinear finite element analysis: methodology and application. *Eng Fail Anal* 80:386–402. <https://doi.org/10.1016/j.engfailanal.2017.07.004>
- Pentecost A (2005) *Travertine*. 1-446. Springer, Berlin. <https://doi.org/10.1007/1-4020-3606-X>
- Praticò Y, Holzer S, Ochsendorf J, Flatt R (2020) Post-fire restoration of historic buildings and implications for Notre-Dame de Paris. *Nat Mater* 2020. <https://doi.org/10.1038/s41563-020-0748-y>
- Přikryl R (2001) Some microstructural aspects of strength variation in rocks. *Int J Rock Mech Min Sci* 38:671–682. [https://doi.org/10.1016/S1365-1609\(01\)00031-4](https://doi.org/10.1016/S1365-1609(01)00031-4)
- Rabat Á, Tomás R, Cano M (2021) Advances in the understanding of the role of degree of saturation and water distribution in mechanical behaviour of calcarenites using magnetic resonance imaging technique. *Constr Build Mater* 303124420. <https://doi.org/10.1016/j.conbuildmat.2021.124420>
- Rabat Á, Tomás R, Cano M (2023) Assessing water-induced changes in tensile behaviour of porous limestones by means of uniaxial direct pull test and indirect methods. *Eng Geol* 313. <https://doi.org/10.1016/j.enggeo.2022.106962>
- Rahman T, Sarkar K (2021) Lithological Control on the Estimation of Uniaxial Compressive Strength by the P-Wave Velocity using supervised and unsupervised learning. *Rock Mech Rock Eng* 54(6):3175–3191. <https://doi.org/10.1007/s00603-021-02445-8>
- Resende R, Lamas L, Lemos J, Calçada R (2014) Stress wave propagation test and numerical modelling of an underground complex. *Int J Rock Mech Min Sci* 72:26–36. <https://doi.org/10.1016/j.ijrmms.2014.08.010>
- Rozgonyi-Boissinot N, Khodabandeh MA, Besharatinezhad A, Török Á (2021) Salt weathering and ultrasonic pulse velocity: Condition assessment of salt damaged porous limestone. *IOP Conference Series: Earth and Environmental Science*, 833(1). <https://doi.org/10.1088/1755-1315/833/1/012070>
- Rudenko AP, Namsaraev ZB, Komova AV, Loboda AY, Mandrykina AV, Krashennikov SV, Yatsishina EB (2023) Application of Biogenic Mineral formation for the Preservation of Limestone Masonry at the Eski-Kermen Archeological Site. *Nanobiotechnol Rep* 18(1):141–151. <https://doi.org/10.1134/S2635167623010123>
- Sarout J, Ferjani M, Guéguen Y (2009) A semi-automatic processing technique for elastic-wave laboratory data. *Ultrasonics* 49(4–5):452–458. <https://doi.org/10.1016/j.ultras.2008.12.001>
- Sharma PK, Singh TN (2008) A correlation between P-wave velocity, impact strength index, slake durability index and uniaxial compressive strength. *Bull Eng Geol Environ* 67(1):17–22. <https://doi.org/10.1007/s10064-007-0109-y>
- Shirole D, Hedayat A, Ghazanfari E, Walton G (2020) Evaluation of an Ultrasonic method for damage characterization of Brittle Rocks. *Rock Mech Rock Eng* 53(5):2077–2094. <https://doi.org/10.1007/s00603-020-02045-y>
- Siegesmund S, Török Á (2011) Building stones. In: Siegesmund S, Snethlage R (eds) *Stone in Architecture*, 11–95. Springer, Berlin, Heidelberg. [https://doi.org/10.1007/978-3-642-14475-2\\_2](https://doi.org/10.1007/978-3-642-14475-2_2)
- Török Á (2008) Black crusts on travertine: factors controlling development and stability. *Environ Geol* 56:583–597. <https://doi.org/10.1007/s00254-008-1297-x>
- Török Á, Licha T, Simon K, Siegesmund S (2011) Urban and rural limestone weathering; the contribution of dust to black crust formation. *Environ Earth Sci* 63:675–693
- Uyanik O, Sabbağ N, Uyanik NA, Öncü Z (2019) Prediction of mechanical and physical properties of some sedimentary rocks from ultrasonic velocities. *Bull Eng Geol Environ* 78(8):6003–6016. <https://doi.org/10.1007/s10064-019-01501-6>
- Vasanelli E, Colangioli D, Calia A, Sileo M, Aiello MA (2015) Ultrasonic pulse velocity for the evaluation of physical and mechanical properties of a highly porous building limestone. *Ultrasonics* 60:33–40. <https://doi.org/10.1016/j.ultras.2015.02.010>
- Vasconcelos G, Lourenço PB, Alves CAS, Pamplona J (2008) Ultrasonic evaluation of the physical and mechanical properties of granites. *Ultrasonics* 48(5):453–466. <https://doi.org/10.1016/j.ultras.2008.03.008>
- Wang Q, Ji S, Sun S, Marcotte D (2009) Correlations between compressional and shear wave velocities and corresponding Poisson's ratios for some common rocks and sulfide ores. *Tectonophysics* 469(1–4):61–72. <https://doi.org/10.1016/j.tecto.2009.01.025>
- Wang B, Hao J, Liu S, Zhou F, Zhang Z, Zhang H, Sun H (2019) Experimental study on the Effect of Gas pressure on Ultrasonic velocity and anisotropy of Anthracite. *Geofluids* 2019. <https://doi.org/10.1155/2019/3183816>
- Wilhelm K, Longman J, Orr SA, Viles H (2021) Stone-built heritage as a proxy archive for long-term historical air quality: a study of weathering crusts on three generations of stone sculptures on Broad Street, Oxford. *Sci Total Environ* 759(143916). <https://doi.org/10.1016/j.scitotenv.2020.143916>
- Yang H, Duan HF, Zhu JB (2021) Thermal effect on Compressional Wave Propagation Across fluid-filled rock joints. *Rock Mech Rock Eng* 54(1):455–462. <https://doi.org/10.1007/s00603-020-02254-5>
- Yurikov A, Nourifard N, Pervukhina M, Lebedev M (2019) Laboratory ultrasonic measurements: Shear transducers for compressional waves. *Lead Edge* 38(5):392–399. <https://doi.org/10.1190/tle38050392.1>

**Publisher's Note** Springer Nature remains neutral with regard to jurisdictional claims in published maps and institutional affiliations.